

Title: Somatic nicotinic acetylcholine receptors control the activity of dopamine neurons and reward-related behaviors.

Authors: Romain Durand-de Cuttoli^{1†}, Sarah Mondoloni^{1†}, Fabio Marti¹, Damien Lemoine¹, Jérémie Naudé¹, Thibaut d'Izarny-Gargas¹, Stéphanie Pons², Uwe Maskos², Dirk Trauner³, Richard H. Kramer⁴, Philippe Faure^{1*} and Alexandre Mourot^{1*}.

Affiliations

¹ Sorbonne Université, INSERM, CNRS, Neuroscience Paris Seine - Institut de Biologie Paris Seine (NPS - IBPS), 75005 Paris, France.

² Unité de Neurobiologie Intégrative des Systèmes Cholinergiques, Department of Neuroscience, CNRS UMR 3571, Institut Pasteur, Paris, France.

³ Department of Chemistry, New York University, New York City, New York.

⁴ Department of Molecular and Cell Biology, University of California Berkeley, Berkeley, CA 94720, USA.

† equal contribution

* Correspondence to alexandre.mourot@inserm.fr or philippe.faure@upmc.fr

Keywords

Nicotine; Dopamine; Acetylcholine; Optogenetics; Nicotinic acetylcholine receptors; Azobenzene photoswitches; Photopharmacology; Addiction; Reward; Ventral Tegmental Area

Summary

Dopamine (DA) neurons of the ventral tegmental area (VTA) integrate cholinergic inputs to regulate key functions such as motivation and goal-directed behaviors. Yet the temporal dynamic range and mechanism of action of acetylcholine (ACh) on the modulation of VTA circuits and reward-related behaviors are not known. Here we used a chemical-genetic approach for rapid and precise optical manipulation of nicotinic neurotransmission in VTA neurons *in vivo*. We provide direct evidence that the ACh tone fine-tunes the firing properties of VTA DA neurons through somatic $\beta 2$ -containing ($\beta 2^*$) nicotinic ACh receptors (nAChRs). Furthermore, locally photo-antagonizing these receptors in the VTA was sufficient to reversibly switch nicotine reinforcement on and off. By enabling control of nicotinic transmission in targeted brain circuits, this technology will help unravel the various physiological functions of nAChRs and may assist in the design of novel therapies relevant to neuropsychiatric disorders.

Introduction

Cholinergic neurotransmission provides a widespread and diffuse signal in the brain (Picciotto et al., 2012; Sarter et al., 2009). ACh alters neurotransmitter release from presynaptic terminals and affects neuronal integration and network activity, by acting through two classes of membrane receptors: metabotropic muscarinic receptors and ionotropic nicotinic ACh receptors (nAChRs). nAChRs consist of hetero- and homo-pentameric arrangements of α and β subunits (9 and 3 genes, respectively), yielding a high combinatorial diversity of channel composition, localization and function (Zoli et al., 2015). Nicotinic neuromodulation controls learning, memory and attention, and has been associated with the development of numerous neurological and psychiatric disorders, including epilepsy, schizophrenia, anxiety and nicotine addiction (Taly et al., 2009). Understanding how nAChRs mediate such diverse functions requires tools for controlling nicotinic neurotransmission in defined brain circuits.

ACh is a modulator of the VTA, a midbrain DAergic nucleus key in the processing of reward-related stimuli and in addiction (Di Chiara and Imperato, 1988; Pignatelli and Bonci, 2015; Volkow and Morales, 2015). The pedunculopontine and laterodorsal tegmental nuclei (PPN and LDT) are the two major cholinergic inputs to the VTA (Beier et al., 2015). Optogenetic activation of PPN and LDT neurons modulates the firing patterns of VTA DA cells and reward-associated behaviors (Dautan et al., 2016; Lammel et al., 2012; Xiao et al., 2016), implicating ACh in these processes. Yet, whether ACh directly affects neuronal excitability at the post-synaptic level, or whether it potentiates the release of other neurotransmitters through pre-synaptic nicotinic and muscarinic receptors is not known.

Brain nAChRs are expressed in high densities in the VTA, and in strategic places such as pre-synaptic terminals, somatic and dendritic post-synaptic sites, as well as DA terminals (Changeux, 2010; Zoli et al., 2015). Genetic and pharmacological manipulations have implicated VTA nAChRs in tuning the activity of DA neurons and in mediating the addictive properties of nicotine (Faure et al., 2014; Mameli-Engvall et al., 2006; Maskos et al., 2005; Morel et al., 2014; Naudé et al., 2016; Picciotto et al., 1998; Tapper et al., 2004; Tolu et al., 2013). However, understanding the mechanism by which ACh and nicotine participate in these activities requires to comprehend the spatio-temporal dynamics of nAChRs activation. Genetic manipulations can eliminate specific nAChRs, but they cannot provide kinetic information about the time course of nAChR signals that could be crucial for actuating VTA circuits and goal-oriented behaviors. Moreover, gene knock-out can have unintended consequences, which include compensatory changes in expression of other receptors or channels, homeostatic adaptations and developmental impairments (King et al., 2003). Pharmacological agents allow activation or inhibition of nAChRs, but they diffuse slowly *in vivo*, they have limited subtype specificity and they cannot be targeted to genetically-defined neuronal cell types.

To fill this gap between molecular and circuit knowledge, we have developed the optogenetic pharmacology for rapid and reversible photocontrol of genetically-targeted mammalian neurotransmitter receptors (Kramer et al., 2013). We previously demonstrated light-controllable nAChRs (LinAChRs) in *Xenopus* oocytes, a heterologous expression system (Tochitsky et al., 2012). Here we deployed strategies for acutely and reversibly controlling nicotinic transmission in the VTA in the mammalian brain, *in vivo*. $\beta 2^*$ receptors account for the great majority of VTA nAChRs and are crucial for the pathophysiology of nicotine addiction (Faure et al., 2014; Maskos et al., 2005). We demonstrate acute interruption of nicotinic signaling in the VTA and reveal that endogenous pontine ACh strongly impacts on the firing

patterns of VTA DA neurons. Moreover, we reversibly prevented the induction of nicotine preference in behaving mice by locally photo-antagonizing the effect of nicotine at the level of somatic $\beta 2^*$ nAChRs in the VTA. This approach to optically antagonize neurotransmitter receptors *in vivo* will help sense the different temporal dynamics of ACh concentrations, and unravel the contribution of specific nAChR isoforms to nicotinic neuromodulation of neural circuits and associated behaviors, including drug abuse.

Results

Design and characterization of $\beta 2$ LinAChR

The vast majority of nAChRs in the mouse VTA contains the $\beta 2$ subunit (Faure et al., 2014; Zoli et al., 2015). Therefore, we engineered this subunit to enable installation of light-sensitivity. We transposed the rat $\beta 2E61C$ mutation, used previously in nAChRs expressed in *Xenopus* oocytes (Tochitsky et al., 2012), to the mouse $\beta 2$ subunit to generate a photosensitizable receptor that traffics and functions normally in the mouse brain. The single cysteine-substitution, which is used for the anchoring of the photoswitchable tethered ligand Maleimide-Azobenzene-Homocholine (MAHoCh), faces the agonist binding sites (Fig. 1A). MAHoCh has a photo-isomerizable azobenzene group, flanked on one side with a thiol-reactive maleimide moiety for conjugation to the cysteine, and on the other with a homocholine ligand for competitive antagonism of nAChRs (Figure 1B). In darkness, the azobenzene group adopts the thermally stable, extended *trans* configuration. Illumination with near-UV (e.g. 380 nm) light isomerizes the azobenzene core to the twisted, *cis* configuration. The *cis* isomer reverses to *trans* either slowly in darkness or rapidly in green light (e.g. 500 nm). Receptor activation in response to ACh agonist remained unaltered in darkness after conjugation of MAHoCh to $\beta 2E61C$. However, agonist activation is blocked in 380 nm light, when *cis* MAHoCh occupies the agonist binding pocket (Figure 1C). Photo-control is bi-directional, and antagonism is relieved under 500 nm light when MAHoCh is in its *trans* form.

To verify whether nAChR currents could be photo-controlled, the $\beta 2E61C$ mutant was co-expressed with the WT $\alpha 4$ subunit in Neuro-2a cells (Figure 1D). Cells were treated with MAHoCh and any remaining untethered photoswitch was washed away prior to electrophysiological recordings. As expected, currents evoked by both carbamylcholine (CCh) and nicotine were strongly inhibited under 380 nm light, when tethered *cis* MAHoCh competes with the agonist (Figure 1E). Currents rapidly (< 500 ms) and fully returned to their initial amplitude upon 525 nm light illumination. Repeated light flashes reduced and increased current amplitude without decrement, consistent with photochemical studies showing that azobenzenes are very resistant to photobleaching (Szymański et al., 2013). Spectroscopic measurements show that *cis* MAHoCh reverts to *trans* in darkness, but very slowly, with a half-life of 74 min in solution (Tochitsky et al., 2012). Consistent with this, we found that nAChR responses remained suppressed in darkness for at least ten minutes after a single flash of 380 nm light, but quickly recovered upon illumination with 525 nm light (Figure 1F). Hence LinAChR could be rapidly toggled between its functional and antagonized forms upon brief illumination with the proper

wavelength of light, but could also remain suppressed several minutes in darkness, eliminating the need for constant illumination.

β 2LinAChR enables inhibition of nicotinic currents in VTA DA neurons

We then tested whether nAChR currents could be photo-controlled in VTA DA neurons using β 2LinAChR. The cysteine-mutant β 2 subunit was co-transduced with eGFP in the VTA of WT mice. Four to six weeks after viral infection, transduced coronal slices were treated with MAHoCh, and nicotine-induced currents were recorded from GFP-positive DA neurons (Fig. 2A). VTA DA neurons were identified based on their anatomical localization and electrophysiological properties (Fig S1A), and were confirmed, together with the injection site, in post-hoc immuno-histological analysis (Fig. 2B). Currents evoked by a local puff of nicotine were strongly inhibited under 380 nm light, and fully restored under 525 nm light (Fig. 2C). Photo-inhibition was robust at both low and high concentrations of nicotine, and was absent in non-transduced slices treated with MAHoCh (Fig. 2D). The degree of photo-inhibition was smaller than that observed in heterologous expression system, suggesting that only a subset of β 2* receptors incorporated the cysteine-mutated β 2. Importantly, over-expression of β 2E61C did not significantly affect the amplitude of nicotine-induced currents (Fig. 2E), indicating that the total number of functional nAChRs at the cell surface was unchanged. Moreover, MAHoCh alone had no detectable off-target effect on other endogenous ion channels or on resting or active membrane properties of the cell (Fig. S1B, C), indicating that the effect of light was specific for β 2E61C* nAChRs. Overall, these experiments show that β 2E61C associates with endogenous nAChR subunits in DA neurons, to produce receptors with normal neurophysiological roles, while allowing specific photo-control of nicotinic signaling.

Somatic β 2*nAChRs control the firing patterns of VTA DA neurons

VTA DA neurons show two distinct patterns of electrical activity: tonic, regular-spiking in the low frequency range and transient sequences of high-frequency firing, referred to as bursts (Paladini and Roper, 2014). Bursting activity, which is a crucial signal for behavioral conditioning (Tsai et al., 2009), is under the control of excitatory afferents from the PPN and LDT (Floresco et al., 2003; Lodge and Grace, 2006; Paladini and Roper, 2014). We asked whether endogenous pontine ACh modulates the firing patterns of VTA DA neurons through β 2 nAChRs. Testing this hypothesis required to deploy strategies for acutely manipulating nicotinic transmission *in vivo*, since DA neurons discharge only in pacemaker-like tonic activity in brain slices, due to cholinergic and glutamatergic afferents being severed (Grace and Onn, 1989). To this aim, we used a microdrive multielectrode manipulator (System mini matrix with five channels, Fig. 3A) directly mounted onto the head of an anaesthetized mouse. This system allowed us to stereotaxically deliver the photoswitch and record the spontaneous activity of putative DA (pDA) neurons, while delivering alternating flashes of 390 and 520 nm light in the VTA (Fig. 3A, B). β 2E61C was virally transduced in the VTA of WT mice and recordings were performed three to four weeks after infection. MAHoCh was infused in the VTA at least an hour before starting the electrophysiological recordings, to allow the excess of untethered photoswitch to be cleared. We first found that the spontaneous activity of pDA neurons from WT and transduced animals were not significantly different in darkness (Fig. S2A), indicating that viral

expression of $\beta 2E61C$ did not affect the native physiology of the cells. We then checked whether alternatively switching light between 390 and 520 nm (20 cycles) affected the spontaneous firing of pDA neurons, by calculating the absolute percent of photoswitching (defined as the absolute value of $((\text{Freq}_{520} - \text{Freq}_{390})/\text{Freq}_{390})$). Importantly, we found that switching wavelength impacted the spontaneous firing rate of MAHoCh-treated pDA neurons of transduced animals, but not of control WT animals (Fig. 3C-D), further evidencing that the effect of light is specific to the anchoring of MAHoCh to the $\beta 2$ cysteine mutant.

For transduced animals, only a fraction of pDA neurons responded to light. To separately evaluate responding from non-responding neurons, we set a threshold (15% absolute photoswitching) to exclude 95 % of the control neurons (Fig. 3D). Based on this threshold, about a third (33/93) of the pDA neurons of transduced animals responded to light, compared to 1/22 for control animals. Non-responding neurons probably were either not transduced, or received too little endogenous cholinergic drive. We then compared the activity of each responding pDA neuron under both wavelengths of light, and observed that some neurons responded with increased firing and some with decreased firing. A majority of the neurons (Type 1, 24/33) showed decreased activity under 390 nm (Fig. 3E), and a transient increase upon switching back to 520 nm, consistent with a direct nAChRs antagonism by *cis* MAHoCh and relief from antagonism when MAHoCh is switched to its *trans* state. The increase in current upon relief from antagonism suggests that ambient ACh is present at the surface of pDA neurons, sufficient to maintain nAChRs in an activated state. In addition, bursting activity was significantly reduced in 390 nm light in Type 1 neurons, when $\beta 2^*nAChRs$ were antagonized (Figure 3F). Hence these receptors play a causal role in determining the firing patterns of VTA DA neurons. A smaller fraction of pDA neurons (Type 2, 9/33) showed the opposite profile, i.e. increased activity under 390 nm light compared to 520 nm (Fig. 3G). This observation suggests that extracellular ACh acts on $\beta 2^*nAChRs$ to exert an inhibitory drive on a sub-population of VTA DA neurons, possibly through an indirect network mechanism. In Type 2 pDA neurons, we observed no effect of light on AP bursts (Fig S2B). Altogether, these results indicate that spontaneously-released ACh acts through post-synaptic (i.e. somatic) $\beta 2^*nAChRs$ to bi-directionally modulate the tonic firing, and increase the bursting activity of VTA DA neurons. This excitatory/inhibitory nicotinic drive is consistent with the duality of the responses observed upon optogenetic activation of pontine cholinergic axons (Dautan et al., 2016) and upon nicotine systemic injections (Eddine et al., 2015).

Nicotine increases the activity of VTA DA neurons by activating somatic nAChRs

In WT mice, VTA DA neurons respond to nicotine with a rapid increase in firing frequency and in bursting activity, and these responses are totally absent in $\beta 2^{-/-}$ mice (Maskos et al., 2005). Several pre- and post-synaptic mechanisms have been proposed to explain the effects of nicotine on DA cell firing (Faure et al., 2014; Juarez and Han, 2016). We tested whether blocking post-synaptic $\beta 2LinAChR$ resulted in a decrease response to nicotine in VTA cells. To this aim, VTA DA neurons transduced with $\beta 2E61C$ were recorded *in vivo* using the juxtacellular technique, which enables long, stable recordings and multiple drug injections (Fig 4A, B). Neurons that were successfully filled with neurobiotin were subsequently immunohistologically identified (Fig S3A). We found that the nicotine-induced variation in firing rate was much smaller under 390 nm light, when receptors were antagonized, and illumination with

520 nm light fully restored the initial response (Fig. 4C-D and S3B). Three of seven neurons tested showed spontaneous bursting, and all of these responded to nicotine by a variation in spikes within bursts (SWB) that appeared reduced under 390 nm light. Importantly, the response recorded from transduced animals was similar to that observed in WT animals (Fig S3C, D), further supporting the idea that the basic neurophysiological properties of DA neurons are unaffected by the viral transduction. Altogether, these experiments show that the effect of nicotine can be reversibly blocked with high spatial, temporal and pharmacological precision in defined brain structures, here the VTA.

Blocking somatic nAChRs is sufficient to disrupt preference to nicotine

The VTA is crucial for the motivational properties of many drugs of abuse, including nicotine (Di Chiara and Imperato, 1988; Volkow and Morales, 2015). In rodents, nicotine increases the activity of VTA DA neurons (Mameli-Engvall et al., 2006; Maskos et al., 2005) and boosts DA release in the Nucleus Accumbens (Di Chiara and Imperato, 1988), signaling its reinforcing, rewarding effect. We tested whether optically blocking $\beta 2^*$ nAChRs of the VTA was sufficient to prevent nicotine from producing its reinforcing properties. To this aim we chronically implanted above the transduced VTA a guide cannula for local delivery of the chemical photoswitch and light (Fig. 5A) and subjected mice to a conditioned-place preference (CPP) protocol (Fig. 5B). Proper transduction and placement of the cannula guide were confirmed immunohistochemically (Fig. S4A). Consistent with previous reports (Walters et al., 2006), WT animals showed a significant place preference for nicotine while $\beta 2^{-/-}$ mice did not (Fig. 5C and Fig. S4B). To determine whether nicotine preference could be reversibly photo-controlled in individual animals, CPP tests were conducted with two groups of $\beta 2E61C$ -transduced animals. Pairings were performed first with nicotine and 390 nm light for group 1, and with nicotine and 520 nm light for group 2. Two months after the first CPP test, nicotine pairing was performed with the alternative light condition, i.e. 520 nm light for group 1 and 390 nm light for group 2. For both groups, animals showed preference to nicotine under 520 but not under 390 nm light (Fig. 5D, E). These results cannot be attributed to changes in general activity behavior, since locomotion was not affected by viral transduction or light (Fig. S4C). Altogether, these experiments show that nicotine-CPP can be reversibly switched on and off in the same animal, by manipulating $\beta 2^*$ nAChRs selectively located in somatic compartments of VTA neurons.

Discussion

In this study, we used an optogenetic pharmacology strategy (Kramer et al., 2013) and demonstrated pharmacologically-specific, rapid local and reversible manipulation of brain nAChRs in behaving mice. Classical opsin-based optogenetics aims at turning specific neurons on or off for decoding neural circuits (Kim et al., 2017). Our strategy expands the optogenetic toolbox beyond excitation and inhibition by providing acute interruption of neurotransmission at the post-synaptic level, and provides mechanistic understanding of how specific transmitters and receptors contribute to modulation of circuits and behaviors.

Our method for photosensitizing receptors relies on the covalent attachment of a chemical photoswitch on a cysteine-modified receptor mutant. The photochemical properties of the

azobenzene photoswitch make this strategy ideally suited for reversibly controlling neurotransmitter receptors with high efficacy and at speeds that rival synaptic transmission (Lemoine et al., 2013; Levitz et al., 2013; W.-C. Lin et al., 2015; Szobota et al., 2007). Comparatively, strategies for photosensitizing proteins based on the fusion of light-sensitive modules (Rost et al., 2017) or chromophore assisted light-inactivation (J. Y. Lin et al., 2013; Takemoto et al., 2017) are too slow or irreversible, respectively. Due to the constraints of bioconjugation, *in vivo* use of photoswitch-tethered receptors in mice has been restricted to the eye (Gaub et al., 2014) and to superficial layers of the cerebral cortex (Levitz et al., 2016; Lin et al., 2015). Here we demonstrate rapid on and off control of neuronal nAChRs in deep brain structures and in freely behaving animals. Our data show that photoswitch delivery resulted in an absolute subtype-specificity control of $\beta 2$ *nAChRs, with no apparent off-target effect. Labeling was rapid (minutes) and, due to its covalent nature, persisted for many hours (we have detected strong photosensitization *in vivo* up to 9 hours after treatment). Importantly, due to the thermal stability of MAHoCh, receptor function was unperturbed in darkness, while brief flashes of light were sufficient to bistably toggle LinAChR between its resting and antagonized states.

The cysteine-modified subunit was transduced in the VTA of WT mice. This resulted in a local replacement of the native $\beta 2$ subunit with the cysteine-mutated version, while leaving nicotinic signaling in other brain regions unaffected. Even though the WT $\beta 2$ subunit remained in transduced cells, photoswitch treatment resulted in robust photo-sensitization of cysteine-mutated $\beta 2$ *nAChRs, indicating incorporation into heteromeric receptors. The pool of receptors remained apparently unchanged, most likely because endogenous nAChR subunits (e.g. $\alpha 4$) limit the total number of heteropentamers at the cell surface. Replacing the WT subunit by its cysteine counterpart in a knock-in animal would guarantee complete gene replacement and untouched expression profile. Yet, viral transduction affords the advantage of allowing the engineered receptor to be targeted for expression in specific types of neurons and in defined neuronal circuits. We used this feature to optically control post-synaptic nAChRs at the level of midbrain neurons, while leaving pre-synaptic receptors from various afferents unaffected, which would be impossible with a transgenic animal. Collectively, our results show that $\beta 2E61C$ competes with native subunits to form functional receptors that, once labeled with MAHoCh, retain their natural functions in darkness, and are made photo-controllable.

Cholinergic neurons from PPN and LDT project extensively to the VTA and substantia nigra (Beier et al., 2015) and are thought to form connections with downstream DAergic and GABAergic neurons through non-synaptic volume transmission. Optogenetic activation of cholinergic pontine axons induces post-synaptic currents in VTA DA neurons that have both nicotinic and glutamatergic signatures (Xiao et al., 2016), suggesting that extracellular ACh potentiates glutamate release by activating nAChRs located on axon terminals. Contrasting with this view, we show here that activation of post-synaptic $\beta 2$ nAChRs by endogenous ACh is sufficient to fine tune both the tonic and burst firing modes of VTA DA neurons. Furthermore, our results add temporal and causal considerations to previous genetic studies (Mameli-Engvall et al., 2006; Tolu et al., 2013) by establishing a direct relationship between the activity of post-synaptic $\beta 2$ nAChRs and the firing patterns of VTA DA neurons. The rebound activity that occurred within 500 ms after de-antagonizing LinAChRs indeed suggests that, even though cholinergic inputs to the VTA are considered sparse, the extracellular levels of ACh are sufficient to activate a large population of receptors and greatly modify the electrical activity of DA neurons. Moreover, we identified a sub-population of VTA DA neurons that is inhibited

when $\beta 2$ nAChRs are de-antagonized, which suggests multiple functional mechanisms by which the cholinergic brainstem neurons may influence the activity of midbrain DA neurons. These results are coherent with the growing body of evidence that show that VTA DA neurons are heterogeneous in their physiological properties (Morales and Margolis, 2017; Yang et al., 2017) and in their responses to drugs (Juarez and Han, 2016), including nicotine (Eddine et al., 2015).

The rewarding properties of nicotine, and especially reinforcement during the acquisition phase of addiction, implicate an elevation of DA in the nucleus accumbens (Di Chiara and Imperato, 1988). Nicotine administration directly depolarizes and activates VTA DA neurons and, consequently, increases extracellular striatal DA (Maskos et al., 2005; Tolu et al., 2013). Nicotine can also induce DA release through pre-synaptic effects, either directly in the striatum at the level of DA terminals (Rice and Cragg, 2004), or within the VTA at the level of GABAergic and glutamatergic afferent terminals (Mansvelder et al., 2002). These different studies suggest alternative circuit mechanisms to explain the outcome of nicotine action on VTA circuitry, for reviews see (Faure et al., 2014; Juarez and Han, 2016). To unravel the distinct roles of somato-dendritic versus terminal receptors, we took advantage of the anatomical and cellular resolution of our approach, and locally blocked the effect of nicotine post-synaptically while leaving pre-synaptic receptors (inside and outside VTA) unaffected. Our results show that somato-dendritic $\beta 2$ *nAChRs of VTA neurons are the main players of both the response to nicotine at the cellular level, and the rewarding properties of this addictive substance at the behavioral level. Importantly, blocking the excitatory phasic input produced by nicotine was sufficient to completely prevent reinforcement learning. This is consistent with our results concerning the ability of $\beta 2$ nAChRs to tune burst firing in DA neurons, and with the fact that activation of LDT-to-VTA cholinergic neurons causes positive reinforcement (Dautan et al., 2016; Xiao et al., 2016). All together, these results strongly suggest that these receptors have a central role in reward processing.

There is a considerable interest to target specific nAChRs and specific circuits to treat psychiatric disorders such as addiction, depression or schizophrenia. Yet, we do not know which native receptor subtype mediates specific physiological or pathological function, hampering development of clinically effective drugs, notably for preventing or treating addiction. Optogenetic pharmacology offers the unique opportunity to locally and reversibly “knock-out” the function of a specific receptor isoform *in vivo*, and to directly evaluate within the same animal the consequences at the cellular, circuit and behavioral levels. Our approach should be applicable to other photo-activatable and -inhibitable nAChR subtypes and other neuronal circuits, and may provide a platform for examining new translational strategies for treating neuropsychiatric disorders.

Acknowledgments

Authors would like to thank Nadine Mouttajagane, Ambre Bonnet and Michael Martin for molecular biology work, and Justine Hadjerici, Claire Nguyen, Steve Didienne and Samir Takillah for their help with electrophysiology and behavior experiments. This work was supported by the Agence Nationale de la Recherche (ANR-JCJC 2014 to A.M.), by a NARSAD Young Investigator Grant from the Brain & Behavior Research Foundation (to A.M.), by the Fondation pour la Recherche Médicale (Équipe FRM DEQ2013326488 to P.F.), by the French National Cancer Institute Grant TABAC-16-022 (to P.F.) and by the Labex Biopsy. A.M. was

recipient of a fundamental research prize from the Medisite Foundation for Neuroscience. R.D.C. was supported by a Ph.D. fellowship from the DIM Cerveau & Pensée program of the Région Ile-de-France, and by a fourth-year PhD fellowship from FRM (FDT20170437427). D.L. was recipient of a Labex Biopsy post-doctoral fellowship. RHK was supported by grants from the NIH (U01-NS090527 and R01-NS100911). P.F. and A.M. laboratory is part of the École des Neurosciences de Paris Ile-de-France RTRA network. P.F. is member of LabEx Bio-Psy and of DHU Pepsy.

Author contribution

A.M., P.F., R.D.C., S.M. and F.M. designed the experiments. A.M. performed molecular biology. R.D.C. and A.M. performed viral injections and cannula implantations. S.M. and D.L. performed cell culture and *in vitro* electrophysiology. S.M., R.D.C., A.M., and T.I.G. performed slice patch-clamp experiments. R.D.C. and F.M. performed *in vivo* electrophysiology. R.D.C. performed behavioral studies. S.M. and R.D.C. performed immunochemistry. R.D.C., S.M., F.M. and J.N. analyzed data. D.T., R.H.K., S.P. and U.M. provided genetic and photochemical tools. A.M., R.D.C., S.M. and R.H.K. wrote the paper, with inputs from P.F., F.M. and J.N.. A.M. and P.F. supervised the work.

Declaration of interests

The authors declare no competing interests

References

- Avale, M.E., Faure, P., Pons, S., Robledo, P., Deltheil, T., David, D.J., Gardier, A.M., Maldonado, R., Granon, S., Changeux, J.-P., Maskos, U., 2008. Interplay of beta2* nicotinic receptors and dopamine pathways in the control of spontaneous locomotion. *Proceedings of the National Academy of Sciences* 105, 15991–15996. doi:10.1073/pnas.0807635105
- Beier, K.T., Steinberg, E.E., DeLoach, K.E., Xie, S., Miyamichi, K., Schwarz, L., Gao, X.J., Kremer, E.J., Malenka, R.C., Luo, L., 2015. Circuit Architecture of VTA Dopamine Neurons Revealed by Systematic Input-Output Mapping. *Cell* 162, 622–634. doi:10.1016/j.cell.2015.07.015
- Changeux, J.-P., 2010. Nicotine addiction and nicotinic receptors: lessons from genetically modified mice. *Nat Rev Neurosci* 11, 389–401. doi:10.1038/nrn2849
- Dautan, D., Souza, A.S., Huerta-Ocampo, I., Valencia, M., Assous, M., Witten, I.B., Deisseroth, K., Tepper, J.M., Bolam, J.P., Gerdjikov, T.V., Mena-Segovia, J., 2016. Segregated cholinergic transmission modulates dopamine neurons integrated in distinct functional circuits. *Nature Neuroscience* 19, 1025–1033. doi:10.1038/nn.4335
- Di Chiara, G., Imperato, A., 1988. Drugs abused by humans preferentially increase synaptic dopamine concentrations in the mesolimbic system of freely moving rats. *PNAS* 85, 5274–5278.
- Eddine, R., Valverde, S., Tolu, S., Dautan, D., Hay, A., Morel, C., Cui, Y., Lambolez, B., Venance, L., Marti, F., Faure, P., 2015. A concurrent excitation and inhibition of dopaminergic subpopulations in response to nicotine. *Sci. Rep.* 5, 8184.

doi:10.1038/srep08184

- Faure, P., Tolu, S., Valverde, S., Naudé, J., 2014. Role of Nicotinic Acetylcholine Receptors in Regulating Dopamine Neuron Activity. *Neuroscience* 282, 86–100.
doi:10.1016/j.neuroscience.2014.05.040
- Floresco, S.B., West, A.R., Ash, B., Moore, H., Grace, A.A., 2003. Afferent modulation of dopamine neuron firing differentially regulates tonic and phasic dopamine transmission. *Nature Neuroscience* 6, 968–973. doi:10.1038/nn1103
- Gaub, B.M., Berry, M.H., Holt, A.E., Reiner, A., Kienzler, M.A., Dolgova, N., Nikonov, S., Aguirre, G.D., Beltran, W.A., Flannery, J.G., Isacoff, E.Y., 2014. Restoration of visual function by expression of a light-gated mammalian ion channel in retinal ganglion cells or ON-bipolar cells. *Proceedings of the National Academy of Sciences* 111, E5574–83.
doi:10.1073/pnas.1414162111
- Grace, A.A., Bunney, B.S., 1984. The control of firing pattern in nigral dopamine neurons: burst firing. *J. Neurosci.* 4, 2877–2890.
- Grace, A.A., Onn, S.P., 1989. Morphology and electrophysiological properties of immunocytochemically identified rat dopamine neurons recorded in vitro. *J. Neurosci.* 9, 3463–3481.
- Juarez, B., Han, M.-H., 2016. Diversity of Dopaminergic Neural Circuits in Response to Drug Exposure. *Neuropsychopharmacology* 1–23. doi:10.1038/npp.2016.32
- Kim, C.K., Adhikari, A., Deisseroth, K., 2017. Integration of optogenetics with complementary methodologies in systems neuroscience. *Nat Rev Neurosci* 18, 222–235.
doi:10.1038/nrn.2017.15
- King, S.L., Marks, M.J., Grady, S.R., Caldarone, B.J., Koren, A.O., Mukhin, A.G., Collins, A.C., Picciotto, M.R., 2003. Conditional expression in corticothalamic efferents reveals a developmental role for nicotinic acetylcholine receptors in modulation of passive avoidance behavior. *J. Neurosci.* 23, 3837–3843.
- Kramer, R.H., Mouro, A., Adesnik, H., 2013. Optogenetic pharmacology for control of native neuronal signaling proteins. *Nature Neuroscience* 16, 816–823. doi:10.1038/nn.3424
- Lammel, S., Hetzel, A., Häckel, O., Jones, I., Liss, B., Roeper, J., 2008. Unique Properties of Mesoprefrontal Neurons within a Dual Mesocorticolimbic Dopamine System. *Neuron* 57, 760–773. doi:10.1016/j.neuron.2008.01.022
- Lammel, S., Lim, B.K., Ran, C., Huang, K.W., Betley, M.J., Tye, K.M., Deisseroth, K., Malenka, R.C., 2012. Input-specific control of reward and aversion in the ventral tegmental area. *Nature* 491, 212–217. doi:10.1038/nature11527
- Lemoine, D., Durand-de Cuttoli, R., Mouro, A., 2016. Optogenetic Control of Mammalian Ion Channels with Chemical Photoswitches. *Methods Mol. Biol.* 1408, 177–193.
doi:10.1007/978-1-4939-3512-3_12
- Lemoine, D., Habermacher, C., Martz, A., Mery, P.-F., Bouquier, N., Diverchy, F., Taly, A., Rassendren, F., Specht, A., Grutter, T., 2013. Optical control of an ion channel gate. *Proceedings of the National Academy of Sciences* 110, 20813–20818.
doi:10.1073/pnas.1318715110
- Levitz, J., Pantoja, C., Gaub, B., Janovjak, H., Reiner, A., Hoagland, A., Schoppik, D., Kane, B., Stawski, P., Schier, A.F., Trauner, D., Isacoff, E.Y., 2013. Optical control of metabotropic glutamate receptors. *Nature Neuroscience*. doi:10.1038/nn.3346
- Lin, J.Y., Sann, S.B., Zhou, K., Nabavi, S., Proulx, C.D., Malinow, R., Jin, Y., Tsien, R.Y., 2013. *NeuroResource*. *Neuron* 79, 241–253. doi:10.1016/j.neuron.2013.05.022

- Lin, W.-C., Tsai, M.-C., Davenport, C.M., Smith, C.M., Veit, J., Wilson, N.M., Adesnik, H., Kramer, R.H., 2015. A Comprehensive Optogenetic Pharmacology Toolkit for In Vivo Control of GABA(A) Receptors and Synaptic Inhibition. *Neuron* 88, 879–891. doi:10.1016/j.neuron.2015.10.026
- Lodge, D.J., Grace, A.A., 2006. The laterodorsal tegmentum is essential for burst firing of ventral tegmental area dopamine neurons. *Proceedings of the National Academy of Sciences* 103, 5167–5172. doi:10.1073/pnas.0510715103
- Mameli-Engvall, M., Evrard, A., Pons, S., Maskos, U., Svensson, T.H., Changeux, J.-P., Faure, P., 2006. Hierarchical control of dopamine neuron-firing patterns by nicotinic receptors. *Neuron* 50, 911–921. doi:10.1016/j.neuron.2006.05.007
- Mansvelder, H.D.H., Keath, J.R.J., McGehee, D.S.D., 2002. Synaptic Mechanisms Underlie Nicotine-Induced Excitability of Brain Reward Areas. *Neuron* 33, 15–15. doi:10.1016/S0896-6273(02)00625-6
- Marx, M., Günter, R.H., Hucko, W., Radnikow, G., Feldmeyer, D., 2012. Improved biocytin labeling and neuronal 3D reconstruction. *Nat Protoc* 7, 394–407. doi:10.1038/nprot.2011.449
- Maskos, U., Molles, B.E., Pons, S., Besson, M., Guiard, B.P., Guilloux, J.P., Evrard, A., Cazala, P., Cormier, A., Mameli-Engvall, M., Dufour, N., Cloëz-Tayarani, I., Bemelmans, A.P., Mallet, J., Gardier, A.M., David, V., Faure, P., Granon, S., Changeux, J.-P., 2005. Nicotine reinforcement and cognition restored by targeted expression of nicotinic receptors. *Nature* 436, 103–107. doi:10.1038/nature03694
- Morales, M., Margolis, E.B., 2017. Ventral tegmental area: cellular heterogeneity, connectivity and behaviour. *Nat Rev Neurosci* 18, 73–85. doi:10.1038/nrn.2016.165
- Morales-Perez, C.L., Noviello, C.M., Hibbs, R.E., 2016. X-ray structure of the human $\alpha 4\beta 2$ nicotinic receptor. *Nature* 538, 411–415. doi:10.1038/nature19785
- Morel, C., Fattore, L., Pons, S., Hay, Y.A., Marti, F., Lambolez, B., De Biasi, M., Lathrop, M., Fratta, W., Maskos, U., Faure, P., 2014. Nicotine consumption is regulated by a human polymorphism in dopamine neurons. *Mol Psychiatry* 19, 930–936. doi:10.1038/mp.2013.158
- Naudé, J., Tolu, S., Dongelmans, M., Torquet, N., Valverde, S., Rodriguez, G., Pons, S.E.P., Maskos, U., Mourot, A., Marti, F., Faure, P., 2016. Nicotinic receptors in the ventral tegmental area promote uncertainty-seeking. *Nature Neuroscience* 1–12. doi:10.1038/nn.4223
- Paladini, C.A., Roeper, J., 2014. Generating bursts (and pauses) in the dopamine midbrain neurons. *Neuroscience* 282, 109–121. doi:10.1016/j.neuroscience.2014.07.032
- Picciotto, M.R., Higley, M.J., Mineur, Y.S., 2012. Acetylcholine as a neuromodulator: cholinergic signaling shapes nervous system function and behavior. *Neuron* 76, 116–129. doi:10.1016/j.neuron.2012.08.036
- Picciotto, M.R., Zoli, M., Léna, C., Bessis, A., Lallemand, Y., Le Novère, N., Vincent, P., Pich, E.M., Brûlet, P., Changeux, J.-P., 1995. Abnormal avoidance learning in mice lacking functional high-affinity nicotine receptor in the brain. *Nature* 374, 65–67. doi:10.1038/374065a0
- Picciotto, M.R., Zoli, M., Rimondini, R., Léna, C., Marubio, L.M., Pich, E.M., Fuxe, K., Changeux, J.-P., 1998. Acetylcholine receptors containing the beta2 subunit are involved in the reinforcing properties of nicotine. *Nature* 391, 173–177. doi:10.1038/34413
- Pignatelli, M., Bonci, A., 2015. Role of Dopamine Neurons in Reward and Aversion: A Synaptic Plasticity Perspective. *Neuron* 86, 1145–1157. doi:10.1016/j.neuron.2015.04.015

- Pinault, D., 1996. A novel single-cell staining procedure performed in vivo under electrophysiological control: morpho-functional features of juxtacellularly labeled thalamic cells and other central neurons with biocytin or Neurobiotin. *Journal of Neuroscience Methods* 65, 113–136.
- Rice, M.E., Cragg, S.J., 2004. Nicotine amplifies reward-related dopamine signals in striatum. *Nature Neuroscience* 7, 583–584. doi:10.1038/nm1244
- Rost, B.R., Schneider-Warme, F., Schmitz, D., Hegemann, P., 2017. Optogenetic Tools for Subcellular Applications in Neuroscience. *Neuron* 96, 572–603. doi:10.1016/j.neuron.2017.09.047
- Sarter, M., Parikh, V., Howe, W.M., 2009. Phasic acetylcholine release and the volume transmission hypothesis: time to move on. *Nat Rev Neurosci* 10, 383–390. doi:10.1038/nrn2635
- Szobota, S., Gorostiza, P., Del Bene, F., Wyart, C., Fortin, D.L., Kolstad, K.D., Tulyathan, O., Volgraf, M., Numano, R., Aaron, H.L., Scott, E.K., Kramer, R.H., Flannery, J.G., Baier, H., Trauner, D., Isacoff, E.Y., 2007. Remote Control of Neuronal Activity with a Light-Gated Glutamate Receptor. *Neuron* 54, 535–545. doi:10.1016/j.neuron.2007.05.010
- Szymański, W., Beierle, J.M., Kistemaker, H.A.V., Velema, W.A., Feringa, B.L., 2013. Reversible Photocontrol of Biological Systems by the Incorporation of Molecular Photoswitches. *Chem. Rev.* 113, 6114–6178. doi:10.1021/cr300179f
- Takemoto, K., Iwanari, H., Tada, H., Suyama, K., Sano, A., Nagai, T., Hamakubo, T., Takahashi, T., 2017. Optical inactivation of synaptic AMPA receptors erases fear memory. *Nature Biotechnology* 35, 38–47. doi:10.1038/nbt.3710
- Taly, A., Corringer, P.-J., Guedin, D., Lestage, P., Changeux, J.-P., 2009. Nicotinic receptors: allosteric transitions and therapeutic targets in the nervous system. *Nat Rev Drug Discov* 8, 733–750. doi:10.1038/nrd2927
- Tapper, A.R., McKinney, S.L., Nashmi, R., Schwarz, J., Deshpande, P., Labarca, C., Whiteaker, P., Marks, M.J., Collins, A.C., Lester, H.A., 2004. Nicotine activation of $\alpha 4^*$ receptors: sufficient for reward, tolerance, and sensitization. *Science* 306, 1029–1032. doi:10.1126/science.1099420
- Tochitsky, I., Banghart, M.R., Mourot, A., Yao, J.Z., Gaub, B., Kramer, R.H., Trauner, D., 2012. Optochemical control of genetically engineered neuronal nicotinic acetylcholine receptors. *Nature Chemistry* 4, 105–111. doi:10.1038/nchem.1234
- Tolu, S., Eddine, R., Marti, F., David, V., Graupner, M., Pons, S., Baudonnat, M., Husson, M., Besson, M., Reperant, C., Zemdegs, J., Pagès, C., Hay, Y.A.H., Lambolez, B., Caboche, J., Gutkin, B., Gardier, A.M., Changeux, J.-P., Faure, P., Maskos, U., 2013. Co-activation of VTA DA and GABA neurons mediates nicotine reinforcement. *Mol Psychiatry* 18, 382–393. doi:10.1038/mp.2012.83
- Tsai, H.-C., Zhang, F., Adamantidis, A.R., Stuber, G.D., Bonci, A., de Lecea, L., Deisseroth, K., 2009. Phasic firing in dopaminergic neurons is sufficient for behavioral conditioning. *Science* 324, 1080–1084. doi:10.1126/science.1168878
- Volkow, N.D., Morales, M., 2015. The Brain on Drugs: From Reward to Addiction. *Cell* 162, 712–725. doi:10.1016/j.cell.2015.07.046
- Walters, C.L., Brown, S., Changeux, J.-P., Martin, B., Damaj, M.I., 2006. The beta2 but not alpha7 subunit of the nicotinic acetylcholine receptor is required for nicotine-conditioned place preference in mice. *Psychopharmacology* 184, 339–344. doi:10.1007/s00213-005-0295-x

- Xiao, C., Cho, J.R., Zhou, C., Treweek, J.B., Chan, K., McKinney, S.L., Bin Yang, Gradinaru, V., 2016. Cholinergic Mesopontine Signals Govern Locomotion and Reward through Dissociable Midbrain Pathways. *Neuron* 90, 333–347. doi:10.1016/j.neuron.2016.03.028
- Xiao, C., Srinivasan, R., Drenan, R.M., Mackey, E.D.W., McIntosh, J.M., Lester, H.A., 2011. Characterizing functional $\alpha 6\beta 2$ nicotinic acetylcholine receptors in vitro: Mutant $\beta 2$ subunits improve membrane expression, and fluorescent proteins reveal responsive cells. *Biochemical Pharmacology* 82, 852–861. doi:10.1016/j.bcp.2011.05.005
- Yang, H., de Jong, J.W., Tak, Y., Peck, J., Bateup, H.S., Lammel, S., 2017. Nucleus Accumbens Subnuclei Regulate Motivated Behavior via Direct Inhibition and Disinhibition of VTA Dopamine Subpopulations. *Neuron* 1–21. doi:10.1016/j.neuron.2017.12.022
- Zoli, M., Pistillo, F., Gotti, C., 2015. Diversity of native nicotinic receptor subtypes in mammalian brain. *Neuropharmacology* 96, 302–311. doi:10.1016/j.neuropharm.2014.11.003

Figure titles and legends

Figure 1. Design and characterization of $\beta 2$ LinAChR. A) Crystal structure of the $\alpha 4\beta 2$ nAChR (PDB ID 5KXI) (Morales-Perez et al., 2016) viewed parallel from the plasma membrane. The $\alpha 4$ subunit is in dark grey and the $\beta 2$ subunit in light grey. The agonist binding sites are located in the extracellular binding domain, at the interface between the α and β subunits. Nicotine (red) and the amino acid E61 (orange) which has been mutated to cysteine in the $\beta 2$ LinAChR are represented as spheres. For clarity, only one $\alpha\beta$ dimer is shown, and an extended view is shown on the right. B) Chemical structure of *trans* and *cis* MAHoCh. The thiol-reactive group maleimide is shown in orange, the azobenzene photo-sensitive moiety in black, and the competitive antagonist homocholine in blue. In darkness, the azobenzene group adopts the thermally stable, extended *trans* configuration. Illumination with near-UV (380 nm) light photo-isomerizes the azobenzene core to the twisted, *cis* configuration. The *cis* isomer reverses to *trans* either slowly in dark conditions ($k_B T$) or rapidly under green light (500 nm). *Cis-trans* photo-isomerization hence results in drastic changes in the geometry and end-to-end distance of MAHoCh. C) Cartoon representation of $\beta 2$ LinAChR. MAHoCh is tethered to $\beta 2E61C$, and the receptor still functions in the dark. Isomerizing the photoswitch back and forth between its *cis* and *trans* forms with two different wavelengths of light enables reversible photocontrol of the receptor: activatable under green light and antagonized under purple light. D) Heterologous co-expression of $\alpha 4$ and $\beta 2E61C$ nAChR subunits in Neuro-2a cells. E) Reversible photocontrol of $\alpha 4\beta 2$ LinAChR in Neuro-2a cells. Currents were recorded in whole-cell voltage-clamp mode at a potential of -60 mV and elicited by an application of CCh (1 mM, 1 s, n = 4) or nicotine (100 μ M, 2 s, n = 5). Currents were strongly inhibited under 380 nm light (71.3 ± 12.5 %, p = 0.038 for CCh and 82.1 ± 4.2 %, p = 0.0082 for nicotine) and fully restored under 525 nm light (p = 0.285 for CCh and 0.125 for nicotine). F) Thermal stability of LinAChR photo-inhibition. After inhibition with 380 nm light, the amplitude of the current remained constant for at least 10 minutes in darkness (p = 1 at t = 12 min), and was restored upon illumination with 525 nm light. All values represent mean \pm SEM.

Figure 2. Reversible photo-inhibition of nAChR currents. A) Viral transduction of the VTA using a lentivirus encoding pGK- $\beta 2E61C$ -IRES-eGFP. B) Immunocytochemical identification of

virally-transduced neurons (GFP-positive) 4 weeks after viral injection. DA neurons are labelled using anti-tyrosine hydroxylase (TH) antibodies. IPN: interpeduncular nucleus, ml: medial lemniscus, SNc: Substantia Nigra pars compacta, SNR: Substantia Nigra pars reticulata, VTA: ventral tegmental area. C) Representative photo-inhibition of nicotine-induced currents (500 μ M, local puff 500 ms) recorded at -60 mV from a GFP-positive DA neuron labeled with MAHoCh (70 μ M, 20 min) in an acute brain slice. D) Average photo-inhibition of nicotinic currents (local puff 500 ms) for 30 μ M (49.5 ± 13.2 %) or 500 μ M nicotine (67.0 ± 4.3 %), recorded as in C) from MAHoCh-treated GFP-positive DA neurons ($n = 6$ and 4 for nicotine 30 and 500 μ M, respectively). Control neurons show no photosensitivity compared to transduced neurons (-6.3 ± 7.7 %, $p = 0.0044$). E) Left: Representative currents induced by nicotine (30 μ M) in a control neuron (Ctrl, grey) and a β 2E61C-transduced neuron (LinAChR, black). Right: Control ($n = 6$) and transduced ($n = 6$) neurons display nicotine-induced currents of same amplitude (-14.5 ± 5.5 and -14.2 ± 4.7 pA, respectively, $p = 0.97$). All values represent mean \pm SEM.

Figure 3. *In vivo* photo-control of endogenous cholinergic signaling. A) Design of the experimental setup for concurrent recording and photocontrol of midbrain DA neurons *in vivo*. A micro-drive system (Mini Matrix) is mounted with a stereotaxic frame on the head of an anesthetized mouse, and enables to position in the VTA one cannula for photoswitch injection, up to three tetrodes for electrophysiological recordings, and one optic fiber connected to a beam combiner for optical stimulation. The photoswitch is injected at least an hour prior to the recordings. B) Representative multi-unit recordings of transduced neurons on two channels of a tetrode while alternating illumination between 390 and 520 nm light. C) Representative electrophysiological response of a MAHoCh-treated control neuron, while alternating illumination conditions between 390 (purple) and 520 nm light (green) every 5 s. Top, raster plot ($n = 19$ transitions) centered on the 390 nm light stimuli, and showing both the 390 to 520 and the 520 to 390 nm light transitions. Bottom, peri-stimulus time histogram (PSTH) of firing frequency using a 250 ms bin. D) Change in firing frequency (expressed in absolute photoswitching) between 390 and 520 nm light for MAHoCh-treated control (Ctrl, light grey, $n = 28$) and β 2E61C-transduced neurons (LinAChR, dark grey, $n = 93$). Photoswitching is calculated as $((\text{Freq}_{520} - \text{Freq}_{390})/\text{Freq}_{390})$ and represented in percent. Cumulative distribution indicates that virally transduced neurons significantly photoswitch compared to controls ($p = 0.0055$, Kolmogorov-Smirnov test). Inset, absolute photoswitching for control neurons (1.87 ± 1.60 %) is lower than that for transduced neurons (21.35 ± 5.90 %). The threshold set at 15% absolute photoswitching (red) was used to determine the fraction of responding neurons in transduced animals ($33/93$, 35.5 %). E) Left, representative electrophysiological response of a virally transduced, MAHoCh-treated type 1 pDA neuron, represented as in C). Right: Average firing rate of all type 1 pDA neurons ($n = 24$), under 520 (green) and 390 nm (purple) light. Firing frequency is significantly lower in 390 nm (1.85 Hz) compared to 520 nm light (3.41 Hz, $p = 1.19 \times 10^{-7}$). F) Top left, raster plot ($n = 20$ transitions) for the spikes contained within bursts (SWB) under 390 nm and 520 nm light, for the same neuron as in E). Bottom left, PSTH of instantaneous SWB frequency using a 250 ms bin. Right, average SWB frequency of all type 1 pDA neurons ($n = 24$), under both wavelengths of light. SWB frequency is significantly lower in 390 compared to 520 nm light ($p = 0.043$). G) Left, representative electrophysiological response of a virally transduced, MAHoCh-treated type 2 pDA neuron, represented as in C). Right: Average firing rate of all type 2 pDA neurons ($n = 9$), under 520 (green) and 390 nm (purple)

light. Firing frequency is significantly higher in 390 nm (5.25 Hz) compared to 520 nm light (3.48 Hz, $p = 0.0039$). All values represent mean \pm SEM

Figure 4. Blocking the effects of nicotine selectively in the VTA. A) Experimental design for photoswitch injection and subsequent juxtacellular recording coupled to photocontrol. B) Representative electrophysiological recording of one VTA DA neuron, during an i.v. injection of nicotine (30 μ g/kg), under 520 (top, green) and 390 nm light (bottom, purple), showing greater electrical activity in green light. C) Representative change in firing frequency (top) and in bursting activity (bottom) of a VTA DA neuron, elicited by an i.v. injection of nicotine (30 μ g/kg), under 390 and 520 nm light, showing reversible photo-inhibition. D) Top, average change in firing rate for VTA DA neurons ($n = 7$) upon nicotine injection under 390 (32.0 %, purple) and 520 nm light (88.8 %, green), normalized to the initial response in darkness. Change in firing frequency in 520 nm light is significantly different for 390 nm ($p = 0.023$, Wilcoxon-Mann-Whitney test with Holm-Bonferroni correction) but not from darkness ($p = 0.81$). Bottom, average change in SWB for bursting VTA DA neurons ($n = 3$) upon nicotine injection under 390 (34.7 %, purple) and 520 nm light (62.4 %, green), normalized to the initial response in darkness. All values represent mean \pm SEM.

Figure 5. Reversibly disrupting nicotine preference. A) Experimental design of the opto-fluidic device for opto-pharmacology experiments in freely-moving mice. The cannula guide is chronically implanted above the VTA and is used for both photoswitch and light delivery. B) Nicotine-place preference protocol. Drug-free pretest (15 min) was followed by 3 consecutive days of pairing, which consisted in morning and evening saline and nicotine (0.5 mg/kg) conditioning sessions (20 min). For experiments using LinAChRs, mice were injected with the photoswitch in the morning and received light (390 or 520 nm, 2 s flashes at 0.1 Hz) in both pairing chambers. On day 5, mice were placed in the central chamber (no drug, no light) and were allowed to freely explore the environment. C) Mean preference score (ps) for WT mice conditioned with saline (grey, $n = 6$, $ps = -12.8 \pm 24.0$ s, $p = 0.69$) and with nicotine (black, $n = 15$, $ps = 165.9 \pm 39.6$ s, $p = 6.1e^{-04}$), and for $\beta 2^{-/-}$ mice conditioned with nicotine (red, $n = 9$, $ps = -16.2 \pm 58.7$ s, $p = 0.44$). D) Representative trajectories of $\beta 2E61C$ -transduced and MAHoCh-treated mice conditioned with nicotine, under 390 (purple) and 520 nm light (green). E) Mean preference for nicotine is abolished under 390 nm (purple, $ps = -17.6 \pm 63.8$ s, $p = 0.80$) and restored under 520 nm light (green, $ps = 227.3 \pm 72.1$ s, $p = 0.015$). Two groups of 7 mice were pooled. All values represent mean \pm SEM.

Material and Methods

Animals

Wild-type male C57BL/6J mice were obtained from Janvier Laboratories (France) and knockout ACNB2 ($\beta 2^{-/-}$) male mice were obtained from Charles Rivers Laboratories (France). $\beta 2^{-/-}$ mice were generated as described previously (Picciotto et al., 1995). All experiments were performed in accordance with the recommendations for animal experiments issued by the European Commission directives 219/1990 and 220/1990, and approved by Université Pierre et Marie Curie.

Chemical photoswitch

MAHoCh was synthesized as described previously (Tochitsky et al., 2012) and was stored as concentrated stock solutions (100 mM) in water-free DMSO at -80°C. For cell labeling, aqueous solutions of MAHoCh were prepared extemporaneously.

Light intensity measurements

Light intensities were measured with a power meter (1916-R, Newport) equipped with a UV-silicon wand detector (818-ST2-DB Newport).

Molecular biology and virus production

The cDNAs for the WT mouse $\beta 2$ and $\alpha 4$ nAChR subunits were from previously-designed pIRES (CMV promoter) or pLenti (pGK promoter) vectors (Maskos et al., 2005). All the constructs are bi-cistronic, with an IRES-eGFP sequence designed to express eGFP and the nAChR subunit using the same promoter. The pLenti construct also contains the long terminal repeats, WPRE and virus elements for packaging into lentiviral vectors. The single cysteine mutation E61C was inserted into pIRES-CMV- $\beta 2$ -IRES-eGFP and pLenti-pGK- $\beta 2$ -IRES-eGFP by site-directed mutagenesis using the Quickchange II XL kit (Agilent). Mutations were verified by DNA sequencing. Lentiviruses were prepared as described previously (Maskos et al., 2005) with a titer of 150 ng of p24 protein in 2 μ l.

Cell culture, transfection and labeling

We used Neuro2A cells, a mouse neuroblastoma cell line classically used for nAChRs expression (Xiao et al., 2011). Briefly, Neuro2A cells were cultured in Dulbecco's Modified Eagle's Medium (DMEM), supplemented with 10% Foetal Bovine Serum (FBS), 1% non-essential amino-acids, 100 units/ml penicillin, 100 mg/ml streptomycin and 2 mM glutamax in a 5 % CO₂ incubator at 37 °C. Cells were transfected overnight with a 1:1 ratio of $\alpha 4$ and $\beta 2$ E61C subunits (pLenti-pGK- $\alpha 4$ -IRES-eGFP and pLenti-pGK- $\beta 2$ E61C-IRES-eGFP), using calcium-phosphate transfection method (Lemoine et al., 2016). Cells were used 2-3 days after transfection for electrophysiology. Prior to recordings, cells were labeled with MAHoCh (20 μ M in external solution) for 20 min.

Stereotaxic viral injections

WT mice (6-8 weeks) were anaesthetized with 1% isoflurane gas and placed in a stereotaxic frame (David Kopf). A small craniotomy was made above the location of the VTA. A lentivirus containing the construct pGK- $\beta 2$ E61C-IRES-eGFP was injected in the VTA (1 μ l at the rate of 0.1 μ l/min) with a 10 μ l syringe (Hamilton) coupled with a polyethylene tubing to a 36 G cannula (Phymep), with the following coordinates [AP: -3.1mm; ML: ± 0.4 mm; DV: -4.7mm from bregma]. Mice were then housed during at least 4 weeks before electrophysiology or behavior experiments.

Midbrain slices preparation and labeling

4-8 weeks after viral infection, mice were deeply anesthetized with an i.p. injection of a mixture of ketamine (150 mg/kg, Imalgene 1000, Merial) and xylazine (60 mg/kg, Rompun 2%, Bayer). Coronal midbrain sections (250 μ m) were sliced using a Compresstome (VF-200; Precisionary Instruments) after intra-cardiac perfusion of cold (0-4°C) sucrose-based artificial cerebrospinal fluid (SB-aCSF) containing (in mM): 125 NaCl, 2.5 KCl, 1.25 NaH₂PO₄, 5.9 MgCl₂, 26

NaHCO₃, 25 Sucrose, 2.5 Glucose, 1 Kynurenate. After 10 min at 35°C for recovery, slices were transferred into oxygenated (95% CO₂/5% O₂) aCSF containing (in mM): 125 NaCl, 2.5 KCl, 1.25 NaH₂PO₄, 2 CaCl₂, 1 MgCl₂, 26 NaHCO₃, 15 Sucrose, 10 Glucose at room temperature for the rest of the day. Slices were labeled individually with MAHoCh (70 μM) in oxygenated aCSF (1 ml) for 20 min, and transferred to a recording chamber continuously perfused at 2 ml/min with oxygenated aCSF.

Patch-clamp recordings

Patch pipettes (5–8 MΩ) were pulled from thin wall borosilicate glass (G150TF-3, Warner Instruments) using a micropipette puller (P-87, Sutter Instruments) and filled with a K-Gluconate based intra-pipette solution containing (in mM): 116 KGlu, 20 HEPES, 0.5 EGTA, 6 KCl, 2 NaCl, 4 ATP, 0.3 GTP and 2 mg/mL biocytin (pH adjusted to 7.2). Cells were visualized using an upright microscope with a Dodt contrast lens and illuminated with a white light source (Scientifica). A 460 nm LED (pE-2, Cooled) was used for visualizing eGFP positive cells (using a bandpass filter cube, AHF). Optical stimulation was applied through the microscope with two LEDs (380 and 525 nm, pE-2, CoolLED), with a light output of 6.5 and 15 mW, corresponding to 5 and 11.7 mW/mm² at the focal plane, respectively. Whole-cell recordings were performed using a patch-clamp amplifier (Axoclamp 200B, Molecular Devices) connected to a Digidata (1550 LowNoise acquisition system, Molecular Devices). Currents were recorded in voltage-clamp mode at -60 mV. Signals were low pass filtered (Bessel, 2 kHz) and collected at 10 kHz using the data acquisition software pClamp 10.5 (Molecular Devices). Electrophysiological recordings were extracted using Clampfit (Molecular Devices) and analyzed with R.

To record nicotinic currents from GFP-positive Neuro2A cells, we used the following external solution (containing in mM): 140 NaCl, 2.8 KCl, 2 CaCl₂, 2 MgCl₂, 10 HEPES, 12 glucose (pH 7.3 with NaOH). We used a computer-controlled, fast-perfusion stepper system (SF-77B, Harvard Apparatus) to apply nicotine-tartrate (100 μM, Sigma-Aldrich) or carbamylcholine chloride (CCh, 1 mM, Sigma-Aldrich), with an interval of 2 min, under different light conditions.

To record nicotinic currents from VTA DA neurons, local puffs (500 ms) of nicotine tartrate (30–500 μM in aCSF) were applied every minute, while alternating wavelengths, using a glass pipette (2–3 μm diameter) positioned 20 to 30 μm away from the soma and connected to a picospritzer (World Precision Instruments, adjusted to ~2 psi). DA neurons were characterized in current clamp mode as described in (Lammel et al., 2008), see Figure S1A. At the end of the recording, the pipette was retracted carefully to allow labeling of the neuron with biocytin (Marx et al., 2012).

In vivo juxtacellular recordings

4–8 weeks after viral infection, mice were deeply anaesthetized with chloral hydrate (8%, 400 mg/kg i.p.), supplemented as required to maintain optimal anesthesia throughout the experimental day. The scalp was opened and a hole was drilled in the skull above the location of the VTA. The saphenous vein was catheterized for intravenous administration of nicotine. Prior to recordings (at least 1 h), 500 nl of a 400 μM solution of MAHoCh in aCSF were injected within the VTA at a rate of 50 nl/min. Extracellular recording electrodes were made from 1.5 mm O.D. / 1.17 mm I.D. borosilicate glass (Harvard Apparatus) using a vertical electrode puller

(Narishige). Under a microscope, the tip was broken to obtain a diameter of 1-2 μm . The electrodes were filled with a 0.5% Na-Acetate solution containing 1.5% of neurobiotin tracer yielding impedances of 20-50 M Ω . Electrophysiological signals were amplified with a headstage (1x, Axon Instruments) coupled to a high-impedance amplifier (Axoclamp-2A, Axon Instruments) and audio monitored (A.M. Systems Inc.). The signal was digitized (Micro-2, Cambridge Electronic Design), sampled at 12.5 kHz and recorded using Spike2 software (CED). DA neurons were sampled in the VTA with the following coordinates: [AP: -3 to -4 mm; ML: +0.3 to +0.6 mm; DV: -4 to -4.8 mm, from Bregma]. Spontaneously active pDA neurons were identified on the basis of previously established electrophysiological criteria: 1) regular firing rate; 2) firing frequency between 1 and 10 Hz; 3) half AP > 1.1 ms. After a baseline recording of at least 5 minutes, a saline solution (0.9% sodium chloride) was injected into the saphenous vein, and after another 10 minutes, injections of nicotine- tartrate (30 $\mu\text{g}/\text{kg}$) were administered via the same route in a final volume of 10 μl and under different light conditions (Dark – 390 nm – 520 nm). Successive injections (up to 6) were performed after the neuron returned to its baseline, or when the firing activity returned stable for at least 3 minutes. Light was applied through an optical fiber (500 μm core, NA = 0.5, Prizmatix) inserted within the glass pipette electrode and coupled through a combiner to 390 / 520 nm ultra-high power LEDs (Prizmatix), yielding an output intensity of 4-8 mW at the tip of the fiber for each wavelength. Light was TTL-controlled and applied 10 s before nicotine injection, for 30 s total. When possible, neurons were electroporated and neurobiotin was expelled from the electrode using positive current pulses as already described (Eddine et al., 2015; Pinault, 1996). Spikes Within Bursts (SWB) were identified as a sequence of spikes with the following features: (1) short intervals, (2) progressively decreasing spike amplitude, and (3) a progressively increasing inter-spike interval (ISI). When considering extracellular recordings, most studies use two criteria to automatically detect bursts: (1) their onset are defined by two consecutive spikes with an interval inferior to 80 ms, whenever (2) they are closed with an interval greater than 160 ms (Grace and Bunney, 1984). Firing rate and %SWB were measured on successive windows of 60 s, with a 45 s overlapping period. Responses to nicotine are presented as the mean percentage of firing frequency or %SWB variation from the baseline \pm SEM. For photoswitching, maximum of firing variation induced by nicotine occurring 200 sec after the injection in purple and green was normalized to the maximum of firing variation in darkness. Spikes were extracted with Spike2 (CED) and analyzed with R (<https://www.r-project.org>).

In vivo multi-unit extracellular recordings

4-8 weeks after viral infection, mice were deeply anaesthetized with chloral hydrate (8%, 400 mg/kg i.p.), supplemented as required to maintain optimal anesthesia throughout the experiment. The scalp was opened and a hole was drilled in the skull above the location of the VTA. We used a MiniMatrix (Fig. 3A, Thomas Recording) allowing us to lower within the VTA: up to 3 tetrodes (Tip shape A, Thomas Recording, Z = 1-2 M Ω), a stainless-steel cannula (OD 120 μm , Thomas Recording) for photoswitch injection and a tip-shaped quartz optical fiber (100 μm core, NA=0.22, Thomas Recording) for photostimulation. The fiber was coupled to a 390/520 nm LED combiner (Prizmatix) with an output intensity of 200-500 μW at the tip of the fiber for both wavelengths. These five elements could be moved independently with micrometer precision. 500 nl of MAHoCh (400 μM in aCSF) were infused (rate: 1 nl/s) within the VTA, and tetrodes were subsequently lowered in the same zone to record neurons. Spontaneously active pDA neurons were recorded at least 30 min after MAHoCh infusion and were identified on the basis of the

electrophysiological criteria used for juxtacellular recordings. The optical fiber was then lowered 100-200 μm above the tetrodes. Baseline activity was recorded for 200 s in darkness, prior to applying 5 s light flashes of alternative wavelengths (390 nm / 520 nm). Electrophysiological signals were acquired with a 20 channels pre-amplifier included in the Mini Matrix (Thomas Recording) connected to an amplifier (Digital Lynx SX 32 channels, Neuralynx) digitized and recorded using Cheetah software (Neuralynx). Spikes were detected using a custom-written Matlab routine and sorted using a classical principal component analysis associated with a cluster cutting method (SpikeSort3D Software, Neuralynx). Neurons were considered as responding when their change in firing rate (% Photoswitching) at the transition from violet to green light exceeded a threshold of 15 %, defined as the maximal % photoswitching observed in controls. This threshold was used for all recorded neurons in every condition. To extract the spikes contained within bursting episodes (SWB) we used the same criteria described in the juxtacellular recordings section. They are represented as the frequency of SWB because of the short analysis window (5 s). All the data were analyzed with R (<https://www.r-project.org>) and Matlab (MathWorks).

Chronic guide cannula implantation

Following stereotaxic viral infection in the VTA (as described above), mice were implanted with a chronic opto-fluid guide cannula (Doric Lenses Inc, Canada, see Fig 4A) using the same coordinates. This guide (length = 3 mm from skull surface, ID/OD = 320/430 μm) has interchangeable threaded connectors and is used either with a fluid injection needle (protruding to 4.8 mm from skull surface) for delivering MAHoCh, or with an optic fiber injector (240 μm core, NA=0.63, protruding to 4.8 mm from skull surface) coupled to a ceramic ferrule (1.25 mm) for light delivery. In-between experiments, a plug is used to close the guide cannula and thus seal the implant. The implant is attached to the skull with a dental cement (SuperBond, Sun Medical).

Nicotine-induced place preference paradigm

The Conditioned Place Preference (CPP) box (Imetronic, France) consists of a Y-maze with one closed arm, and two other arms with manually operated doors. Two rectangular chambers (11x25 cm) with different cues (texture and color), are separated by a center triangular compartment (side of 11 cm). One pairing compartment has grey textured floor and walls and the other one has smooth black and white striped walls and floor. The first day (pretest) of the experiment, mice (n=6-9 animals / group) explored the environment for 900 s (15 min) and the time spent in each compartment was recorded. Pretest data were used to segregate the animals with equal bias so each group has an initial preference score almost null, indicating no preference on average. On day 2, 3 and 4, animals received an i.p. injection of nicotine tartrate (0.5 mg/kg, in PBS) or an equivalent injection of saline (PBS), and immediately confined to one of the pairing chamber for 1200 s (20 min). The CPP test was performed using a single nicotine concentration (0.5 mg/kg) which is known to induce preference in mice (Walters et al., 2006). Groups were balanced so the animals do not always get nicotine in the same chamber. On the evening of the same day, mice received an injection of the alternate solution (nicotine or saline) and were placed in the opposite pairing chamber. The saline control animals received a saline injection in both pairing compartments. On day 5 (test), animals were allowed to explore the whole open-field for 900 s (15 min) and the time spent in each chamber was recorded. The preference score (ps) is expressed in seconds and is calculated by subtracting pretest from test data. Trajectories and time spent on each side are calculated based upon animal detection. Place preference and locomotor

activity were recorded using a video camera, connected to a video-track system, out of sight of the experimenter. A home-made software (Labview 2014, National Instruments) tracked the animal, recorded its trajectory (20 frames per s) for 15 min and sent TTL pulses to the LED controller when appropriate (pairing sessions). For optogenetic pharmacology experiments, MAHoCh (400 μ M in aCSF, 500 nl in 5 minutes) was injected early in the morning of pairing days (2, 3 and 4) under light gas anesthesia (Isoflurane 1%). 520/390 nm light was applied during pairing sessions (day 2, 3 and 4), on both sides, through a patch cord (500 μ m core, NA=0.5, Prizmatix, Israel) connected to the implanted ferrule with a sleeve and to the 390/520 nm combined UHP-LEDs (Prizmatix). Light was applied with the following pattern: 2 s pulses à 0.1 Hz with a measured output intensity of 10 mW at the tip of the patch cord. Light was not applied during pre-test and test. Behavioral data were collected and analyzed using home-made LabVIEW (National Instruments) and Matlab (MathWorks) routines.

Immunohistochemistry

After patch-clamp experiments, individual slices (250 μ m) were transferred in 4 % paraformaldehyde (PFA) for 12-24 hours and then to PBS, and kept at 4°C. At the end of *in vivo* experiments, transduced mice received, under deep anesthesia (Ketamine/Xylazine), an intra-cardiac perfusion of (1) PBS (50 ml) and (2) paraformaldehyde (4% PFA, 50 ml) and brains were rapidly removed and let in 4% PFA for 48-72 h of fixation at 4 °C. Serial 60 μ m sections of the ROI were cut with a vibratome. Immunohistochemistry was performed as follows: Floating VTA brain sections were incubated 1 hour at 4 °C in a solution of phosphate-buffered saline (PBS) containing 3% Bovine Serum Albumin (BSA, Sigma; A4503) and 0.2% Triton X-100 and then incubated overnight at 4 °C with a mouse anti-Tyrosine Hydroxylase antibody (TH, Sigma, T1299) at 1:200 dilution and a rabbit anti-GFP antibody (Molecular Probes, A-6455) at 1:1000 dilution in PBS containing 1.5% BSA and 0.2% Triton X-100. The following day, sections were rinsed with PBS and then incubated 3 h at 22–25 °C with Cy3-conjugated anti-mouse and Cy2-conjugated anti-rabbit secondary antibodies (Jackson ImmunoResearch, 715-165-150 and 711-225-152) at 1:200 and 1/1000 dilution respectively in a solution of 1.5% BSA and 0.2% Triton X-100 in PBS. In the case of biocytin/neurobiotin labelling, TH identification of the neuron was performed using AMCA-conjugated Streptavidin (Jackson ImmunoResearch) at 1:200 dilution. After three rinses in PBS, wet slices were mounted using Prolong Gold Antifade Reagent (Invitrogen, P36930). Microscopy was carried out either with a confocal microscope (Leica) or an epifluorescence microscope (Leica), and images captured using a camera and analyzed with ImageJ software.

Statistical analysis

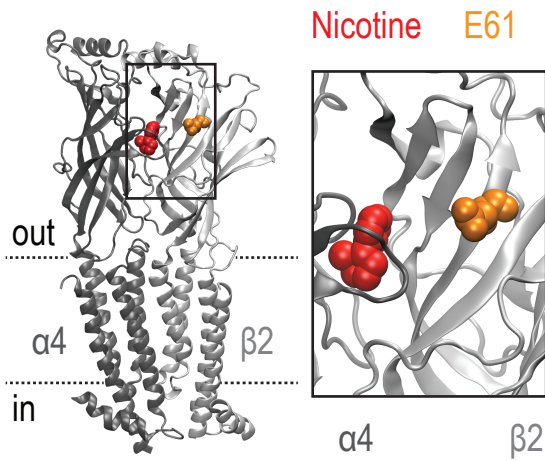
No statistical methods were used to predetermine sample sizes. Data are plotted as mean \pm SEM. Total number (n) of observations in each group and statistics used are indicated in figure and/or figure legend. Comparisons between means were performed using parametric tests (two-sample t-test) when parameters followed a normal distribution (Shapiro test $P > 0.05$), and non-parametric tests (here, Wilcoxon or Mann-Whitney (U-test)) when this was not the case. Homogeneity of variances was tested preliminarily and the t-tests were Welch-corrected if needed. Multiple comparisons were Holm-Bonferroni corrected. Comparison between the cumulative distributions of *in vivo* multi-unit recordings between controls and LinAChRs (Fig.

3D) was performed using a Kolmogorov-Smirnov test. $P > 0.05$ was considered to be not statistically significant.

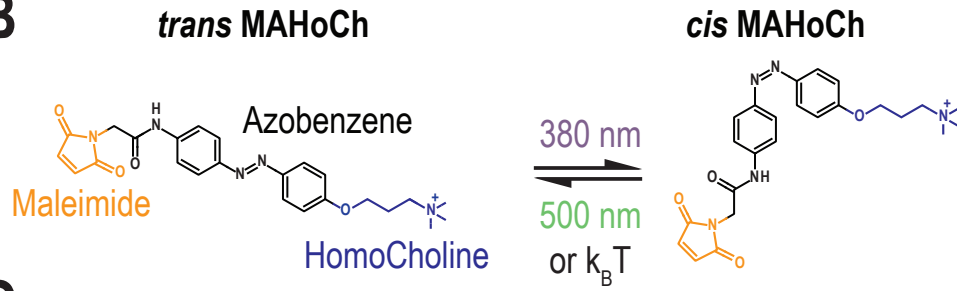
Fig.1

bioRxiv preprint doi: <https://doi.org/10.1101/266163>; this version posted February 15, 2018. The copyright holder for this preprint (which was not certified by peer review) is the author/funder. All rights reserved. No reuse allowed without permission.

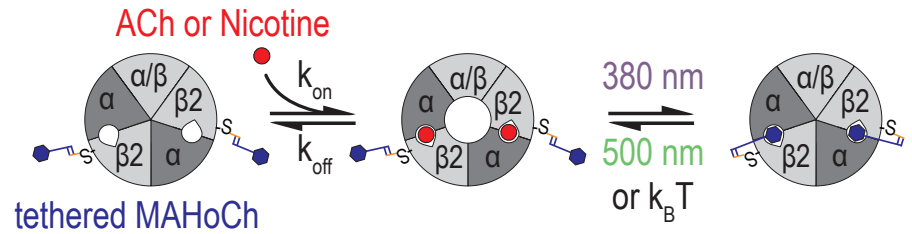
A



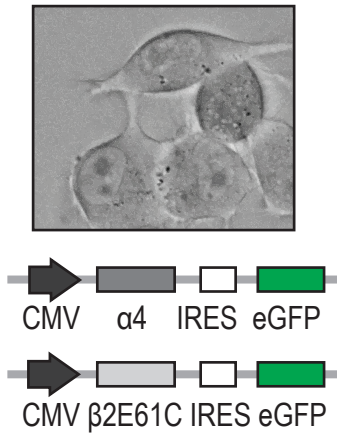
B



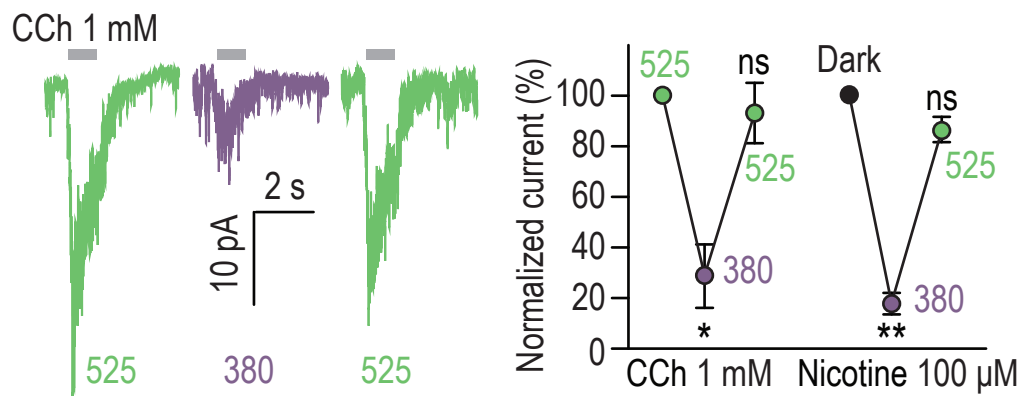
C



D



E



F

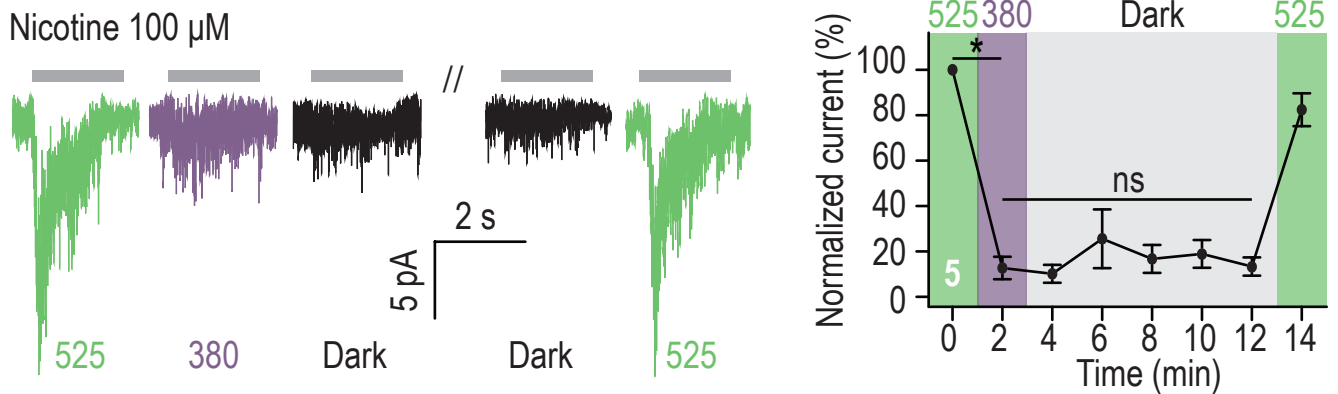
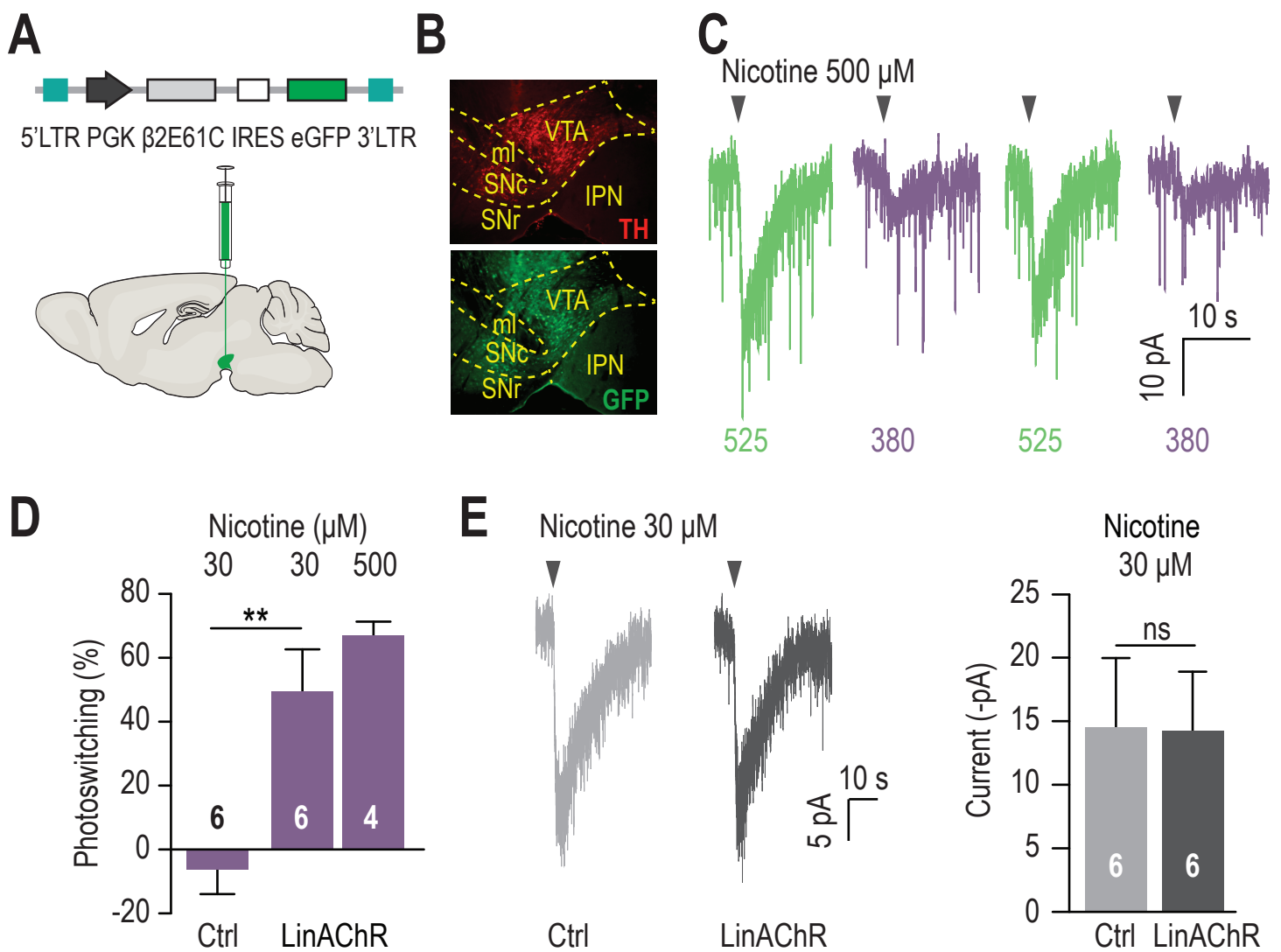


Fig.2



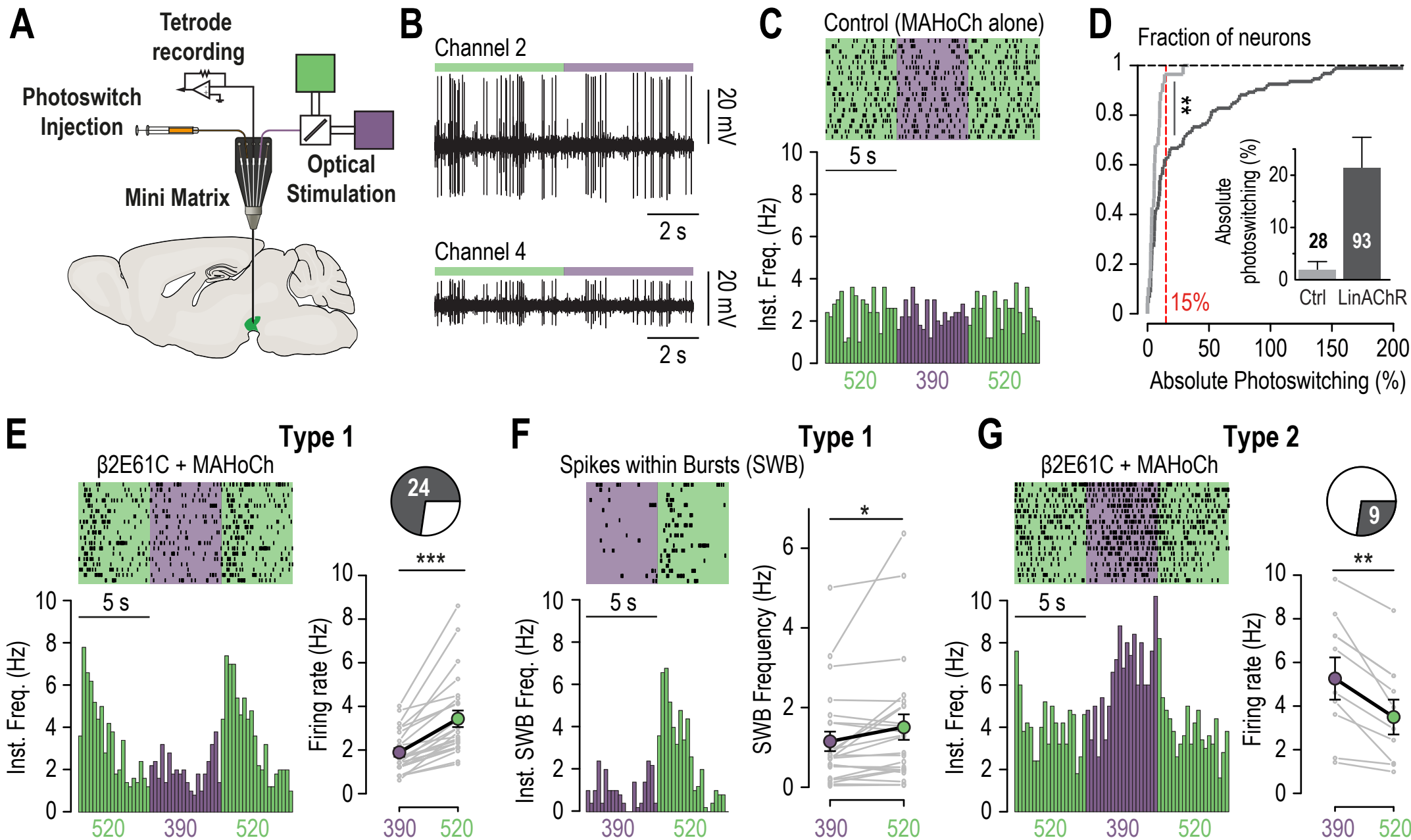


Fig. 3

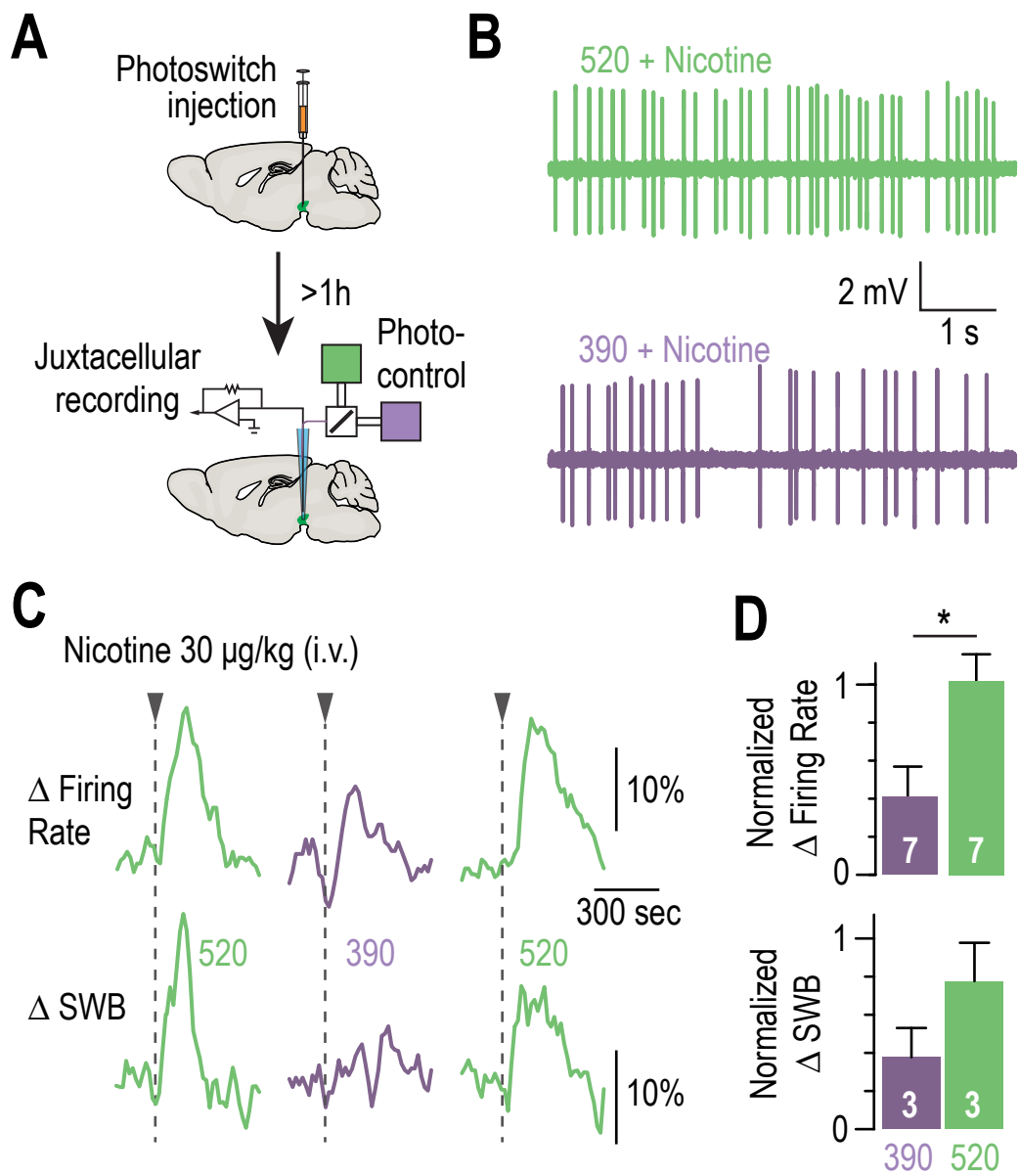


Fig. 4

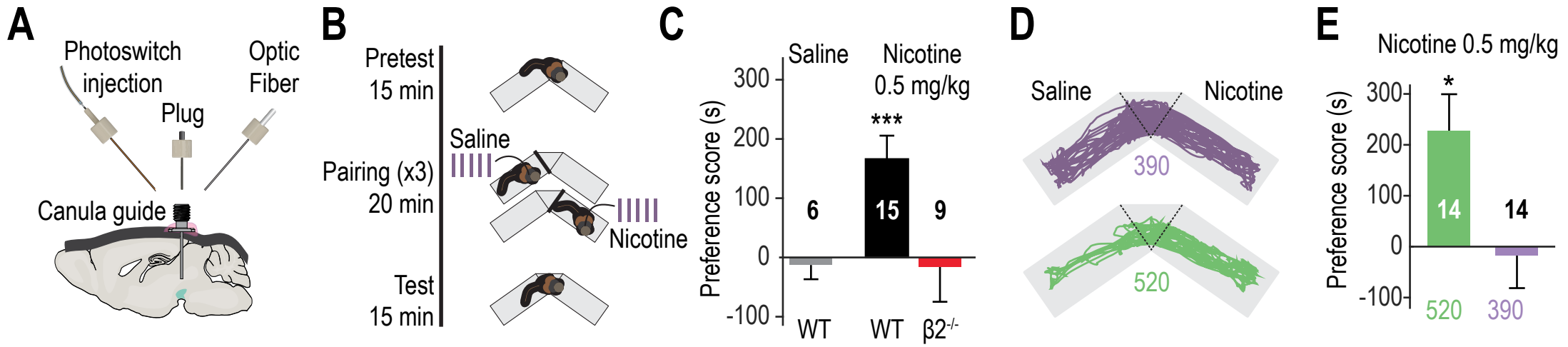


Fig. 5